Gold Bull (2013) 46:103–115
DOI 10.1007/s13404-013-0087-8

ORIGINAL PAPER

Extended reliability of gold and copper ball bonds in microelectronic packaging

Chong Leong Gan · Classe Francis · Bak Lee Chan · Uda Hashim

Published online: 10 April 2013
© The Author(s) 2013. This article is published with open access at SpringerLink.com

Abstract Wire bonding is the predominant mode of interconnection in microelectronic packaging. Gold wire bonding has been refined again and again to retain control of interconnect technology due to its ease of workability and years of reliability data. Copper (Cu) wire bonding is well known for its advantages such as cost-effectiveness and better electrical conductivity in microelectronic packaging. However, extended reliabilities of Cu wire bonding are still unknown as of now. Extended reliabilities of Au and Pd-coated Cu (Cu) ball bonds are useful technical information for Au and Cu wire deployment in microelectronic packaging. This paper discusses the influence of wire type and mold compound effect on the package reliability and after several component reliability stress tests. Failure analysis has been conducted to identify its associated failure mechanisms after the package conditions for Au and Cu ball bonds. Extended reliabilities of both wire types are investigated after unbiased HAST (UHAST), temperature cycling (TC), and high-temperature storage life test (HTSL) at 150, 175, and 200 °C aging temperatures. Weibull plots have been plotted for each reliability stress. Obviously, Au ball bond is found with longer time to failure in unbiased HAST stress compared to Cu ball bonds for both mold compounds. Cu wire exhibits equivalent package and or better reliability margin compared to Au ball bonds in TC and HTSL tests. Failure mechanisms of UHAST and TC have been proposed, and its mean time to failure (t_{50}), characteristic life ($t_{63.2}$, η), and shape parameter (β) have been discussed in this paper. Feasibility of silver (Ag) wire bonding deployment in microelectronic packaging is discussed at the last section in this paper.

Keywords Gold bonding wire · Copper bonding wire · Silver wire · Extended reliability · Microelectronic packaging

C. L. Gan (✉) · C. Francis · B. L. Chan
Spansion (Penang) Sdn. Bhd., Bayan Lepas,
11900 Penang, Malaysia
e-mail: chong-leong.gan@spansion.com

C. L. Gan · U. Hashim
Institute of Nano Electronic Engineering (INEE),
Universiti Malaysia Perlis, 01000 Kangar, Perlis, Malaysia

Introduction

Gold bonding wire has been extensively used for the fabrication of integrated circuits because of its good electrical conductivity and mechanical stability with a diameter of 20 μm or less. With significant increases in gold price, gold ball bonding has become a more costly process that has a considerable economic effect on the assembly of packages used in consumer electronics. An alternative wire material to gold is copper, which is much cheaper, has several technical benefits including better electrical conductivity, and has been widely used in discrete and power devices with wire diameters typically larger than 30 μm in diameter for many years. The potentials and cost considerations of finding an alternative to replace gold wire bonding in microelectronic packaging are driven by new technologies coming to the market [1]. Copper wire bonding appears to be the alternate materials, and various engineering studies on copper wire deployment have been reported [2, 3]. The Au–Al intermetallic compound (IMC) growth is widely characterized and analyzed [4–6]. Zulkifli MN et al. [7] suggested new approaches: examining the effect of individual phase and surroundings on the strengthening produced by the Au–Al intermetallic compound, combining FEA based on friction and wire-bonding parameters, and correlating TEM results with results obtained from other techniques should enable a more detailed understanding of the bondability and strength of thermosonic gold wire bonds. Key technical barriers such as intermetal dielectric cracking due to excessive bonding, copper ball bond corrosion under moist environments, and extended reliability of copper ball bonds are identified accordingly [8–10]. Copper ball bond is

more susceptible to moisture corrosion compared to gold ball bonds and undergoes different corrosion mechanisms in microelectronic packaging [11, 12]. Our previous studies indicate that Pd-coated copper ball bond outperforms gold ball bonds in biased HAST wearout reliability [13]. Extended reliability of high-temperature storage life (HTSL) of copper ball bonds in TSOP package is found with apparent activation energy (E_{aa}) of ~0.70 eV compared to gold ball bonds [14]. Blish et al. [15] investigated E_{aa} of typical Au–Al IMC of 1.0~1.5 eV, which is Al thickness dependent. Hence, extended reliability is crucial to determine the lifetime of gold and copper ball bonds in microelectronic packaging. The Cu–Al and Au–Al IMC growth kinetics were studied, and it was found that Cu–Al growth is at least 5× slower than Au–Al IMC [16]. However, copper wire bonding still pose reliability challenges and complex failure mechanisms which could be the main barriers to entirely replace gold wire bonding [17]. In this study, we have prepared FBGA 64 package assembled with gold and Pd-coated copper wire and load for unbiased HAST (UHAST), temperature cycling (TC), and HTSL tests.

Will Cu or Ag wires entirely replace Au wire bonding?

In general, Cu wire is not an ultimate bonding wire solution in semiconductor packaging. Cu wire bonding is more suitable to be deployed in low-pin-count semiconductor packaging, flash memory packaging, or high-power devices which utilize a larger diameter for bonding wire. The various considerations such as its long-term extended reliability performance and bondpad cratering challenges still pose a showstopper for full sweep of copper wire bonding in semiconductor packaging. Undeniably, the improved N_2 kit (which is installed on wire bonder) will improve the wire-bonding process with an inert environment since Cu wire is vulnerable to corrosion and oxidation in production floor. Cu wire will not entirely replace conventional Au wire bonding in semiconductor packaging but rather another option of packaging methods other than Au, Al, and possibly Ag wire bonding.

Au, Cu, or Ag wire alloys for semiconductor packaging?

Cu as new interconnect material has increasingly gained popularity due its lower cost and good thermal and mechanical properties compared to Au wire. Table 1 shows some general material properties, where the similar mechanical properties of Ag and Au can be seen and Ag is more superior in terms of electrical and thermal conductivity. When compared to Cu, Ag is similar in conductivity, but softer in terms of mechanical properties. These properties will change as it is dependent on the purity of the metals.

Au wire exhibits excellent UHAST extended reliability and more stable assembly processes (in terms of shear strength and wire pull strength in the as-bonded stage). This is the most pivotal deciding factor for keeping Au wire bonding in some of the customer-end field applications such as medical, automotive, and military market segments. Silver (Ag) wire bonding is still a new interconnect method in semiconductor packaging and yet to be widely adopted by major semiconductor companies due to lack of reliability data and further engineering evaluations. Many claims on its advantages of moderate AgAl IMC formation and growth rate, and easier pluck-and-play for mass production are key success factors for Ag wire to replace Au or Cu wire bonding. Cho et al. [18] reported that Pd alloying of the Ag wire was effective in improving the reliability of Ag ball bond. The lifetime in PCT increased with increasing Pd concentration in the Ag wire. Free air ball formation is found better in Ag–Au–Pd compared to 2 N Ag wire alloy [19]. The bonding process of Ag wire bonding is pretty similar to Au wire bonding [20]. Another bondability study is conducted on Au–Ag wire alloy, and caution should be given to bonding temperature and first ball bond parameter setting [22]. This observation convinces the great opportunity of using Ag–Au–Pd alloy instead of bare 2 N Ag wire in microelectronic packaging. Another reliable Ag–8Au–3Pd wire alloy is found with high reliability and low electrical resistivity, which is processed with annealing twins [21, 23, 24]. Bare Ag wire or tertiary Ag alloy (such as Ag–8Au–3Pd or Ag–Au–Pd) are identified as next potential candidates of microelectronic packaging. In a nutshell, Au, Ag, and Cu (bare or Pd-coated Cu) wire alloys will exist as three alternatives of wire-bonding techniques in semiconductor

Table 1 Material properties of bare Ag, Au, and Cu

Material properties	Units	Ag	Au	Cu
Thermal conductivity	W/mK	430	320	400
Electrical resistivity	10^{-8} Ωm	1.63	2.2	1.72
Young's modulus	GPa	83	78	130
Vickers hardness	MPa	251	216	369

Table 2 Summary of experimental matrix (for Au and Cu wires)

Mold compound type	Extended reliability test	Test conditions	Sample size
A	UHAST	85%RH, 130 °C	77
A	TC	-40 to 150 °C	77
A	HTSL	150 °C	45
A	HTSL	175 °C	45
A	HTSL	200 °C	45
B	UHAST	85%RH, 130 °C	77
B	TC	-40 to 150 °C	77
B	HTSL	150 °C	45
B	HTSL	175 °C	45
B	HTSL	200 °C	45

Table 3 Summary of extended reliability results (mold compound types A and B of Au and Cu wires)

Mold compound	Wire type	Test type	Test conditions	t_{first} (h/cyc)	t_{50} (h/cyc)	$t_{63.2}$ (η)	β
A	Cu	UHAST	85%RH, 130 °C	3,000	6,610	7,061	5.53
A	Cu	TC	-40 to 150 °C	9,500	16,756	17,504	7.23
A	Au	UHAST	85%RH, 130 °C	4,000	8,681	9,541	3.67
A	Au	TC	-40 to 150 °C	9,000	15,060	15,691	8.32
B	Cu	UHAST	85%RH, 130 °C	1,248	9,503	11,331	1.92
B	Cu	TC	-40 to 150 °C	11,000	18,175	18,919	8.35
B	Au	UHAST	85%RH, 130 °C	2,000	7,086	7,911	3.22
B	Au	TC	-40 to 150 °C	10,500	15,251	15,251	11.43

packaging based on its customer-end field applications and packaging cost considerations. The packaging cost of Ag wire bonding is moderate and in between of Au and Cu wire bonding.

Future of Au wire bonding in semiconductor packaging

Au wire bonding will still exist in microelectronic packaging in view of its process stability and higher moisture reliability margin compared to recent penetration of Cu wire bonding. The primary motivation for uptake of copper wire bonding is, however, more strongly cost driven rather than motivated by very clear and distinct process, performance, or reliability advantages [3]. In our extended reliability study, Au ball bond exhibits higher UHAST wearout reliability margin compared to Cu ball bonds for epoxy mold compound (EMC) A. This is one of the most important factors to keep Au wire bonding in microelectronic packaging, especially for high-pin-count semiconductor packaging. Cu is known for more susceptible corrosion activity under moist environments. End customers such as automotive, military, and medical industries had expressed concerns over massive transition from Au to Cu wire bonding. Ag wire bonding, however, is not a mature assembly process, and it requires further engineering studies on IMC formation, extended reliability, and test yield analysis on flawless high-volume manufacturing process to validate the feasibility of Ag wire bonding in microelectronic packaging. There is clearly a place for copper (bare copper or Pd-coated copper wire) or silver (bare silver or Ag–Au–Pd alloy) wire bonding in microelectronic packaging, but it is likely that rather than replacing gold wire entirely, copper or silver wire bonding will become another option alongside gold wire bonding which microelectronic package designers can consider for package assembly.

Experimental Procedure

Materials used include 0.8 mil Pd-coated Cu wire (Cu), 4 N (99.99 % purity) gold (Au) wire, and 110-nm flash devices packaged into fortified fine pitch BGA packages, with green (<20 ppm chloride in content) molding compound and substrate. In this Cu wire wearout reliability study, there are a total of four legs comprised of Pd-coated Cu wire and 4 N Au wire bonded on fine pitch 64-ball BGA packages on a 2 L substrate. Sample size used is 77 units for UHAST and TC

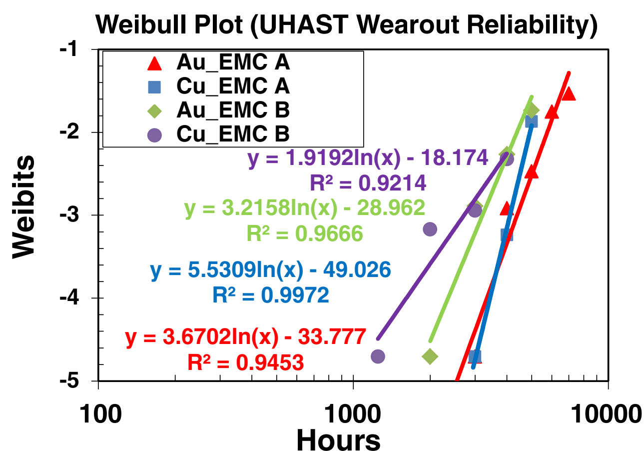

Fig. 1 Extended UHAST reliability plots of Au and Cu ball bonds with different EMCs

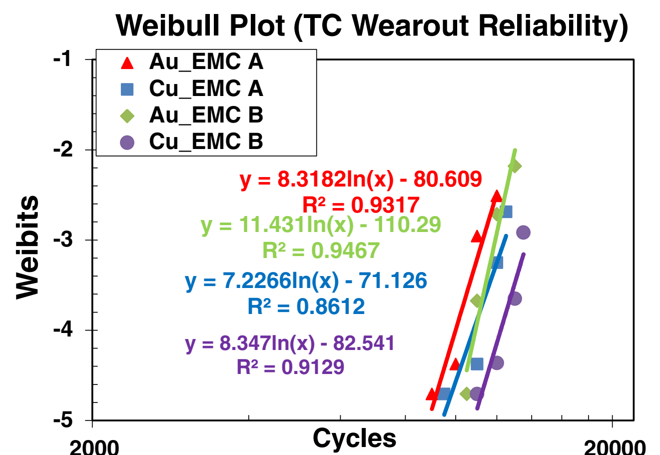

Fig. 2 Extended TC reliability plots of Au and Cu ball bonds with different mold compounds A and B

Table 4 Key material characteristics of EMCs A and B

Material characteristics	Units	EMC A	EMC B
Linear coefficient of thermal expansion 1 (CTE, α_1)	10^{-5}/°C	1.1±0.3	0.7±0.3
Linear coefficient of thermal expansion 2 (CTE, α_2)	10^{-5}/°C	4.5±1.0	3.0±1.0
Glass transition temperature (T_g)	°C	125±15	125±15
Cl^- content	ppm	<10	<10
Na content	ppm	<10	< 10

stresses. The corresponding stress test conditions are tabulated in Table 2. After electrical test, good samples were then subjected for preconditioning and 3 times reflow at 260 °C as described in JEDEC IPC-STD 020 standard, followed by UHAST stress testing per JESD22-A118 at 130 °C/85%RH) [5] and TC per JESD22-A104 at -40 to 150 °C. Electrical testing was conducted after several readpoints of stress as well as to check Au and Cu ball bond integrity in terms of its moisture and thermomechanical reliability.

Another set of materials was used to estimate the apparent activation energies (E_{aa}) of Au and Cu ball bonds assembled with EMC A and EMC B. The key materials used include 0.8 mil Pd-coated Cu wire and 4 N (99.99 % purity) Au wire, fine pitch BGA package, and 110-nm device which is packed in fortified fineline BGA package, green (<20 ppm chloride in content) in molding compound and substrate. All direct material used in this evaluation study for the 110 nm, flash device (with top Al metallization bondpad) for packaging purpose. A total of six legs of 45 units of Au and Pd-coated Cu wire bonded on fine pitch 64-ball BGA packages are subjected to 150, 175, and 200 °C aging temperatures. Electrical testing was conducted after each hour and cycle of stress to check Au and Cu ball bond integrity in terms of its ball bond HTSL reliability with various aging conditions.

Result and Discussion

The extended reliability results of UHAST and TC tests of Cu and Au ball bonds used in encapsulated mold compound types A and B are given in Table 3. All extended reliability curves belong to wearout reliability since its β (shape parameter) is more than 1.0 in all UHAST and TC reliability curves. In reliability testing, t_{first} denotes time to first occurrence of failure in reliability stresses, t_{50} (also known as MTTF) refers to time to failure of 50 % of the tested sample, and $t_{63.2}$ (also known as characteristic life) refers to time to failure of 63.2 % of the tested sample in reliability testing. Mold compound B reveals higher hours and cycles to failure (t_{first}, t_{50}, and $t_{63.2}$) in TC test compared to mold compound A, although they are with pretty similar technical specifications. Au ball bonds

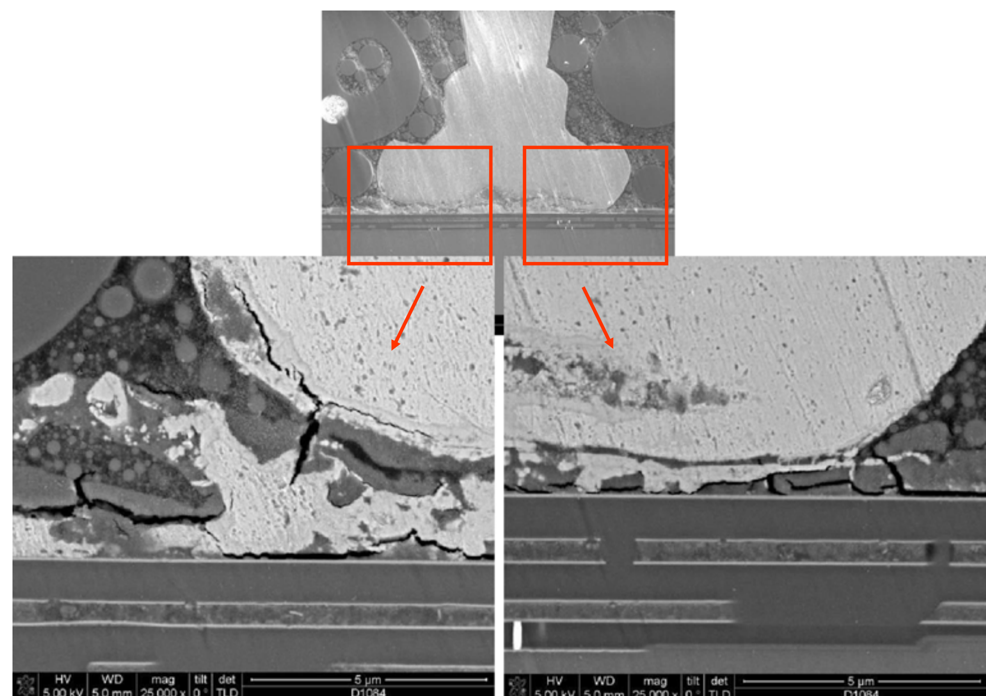

Fig. 3 The representative SEM image shows Cu ball bond microcracking along the Au–Al interface after UHAST 3,000 h

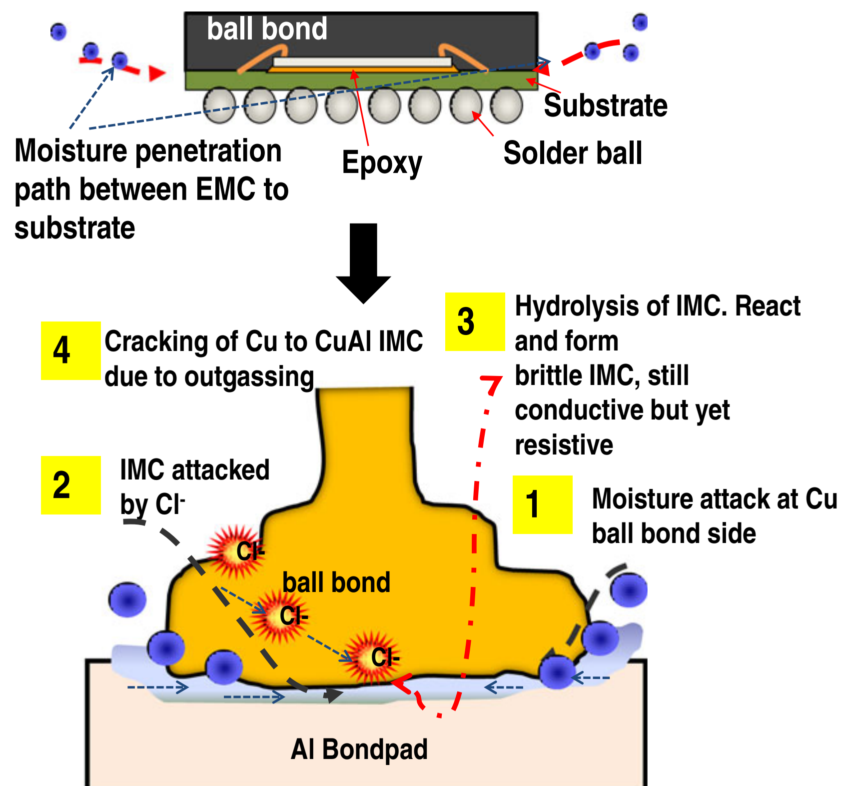

Fig. 4 Proposed UHAST failure mechanism of Cu ball bond

show superior extended UHAST reliability than Cu ball bonds for mold compound A but smaller t_{50} and $t_{63.2}$ for mold compound B (see Fig. 1 and Table 3). This could be due to a more stable Au and the higher corrosion resistance under moisture UHAST conditions compared to Cu ball bonds in mold compound A. The microstructure analysis of Au ball bond after extended UHAST test is shown in Fig. 8.

However, we observed Cu ball bonds with higher TC extended reliability performance (higher t_{first}, t_{50}, and $t_{63.2}$) compared to Au ball bonds in FBGA 64 package of both mold compounds A and B (Fig. 2). The key material characteristics of epoxy mold compounds A and B are given in Table 4. The effect of wire type is not the key factor affecting the TC reliability performance, but we observed a higher extended reliability performance in Cu ball bonds compared to Au ball bonds. Again, the coefficients of thermal expansion (CTE) of mold compounds A and B are pretty similar, except that the CTE is different between Au and Cu to the silicon die. Overall, EMC B (with α_2 of 3.0×10^{-5}/°C which is closer to silicon die CTE of 3.0 ppm/°C compared to EMC A) shows higher TC reliability margin and longer cycles to failure for Au and Cu wires.

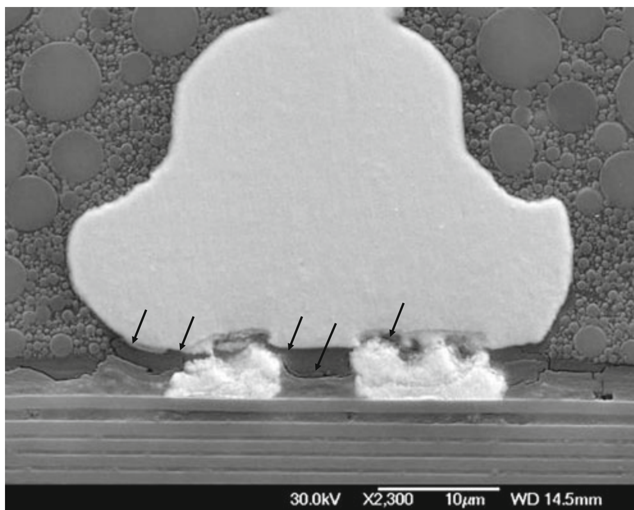

Fig. 5 The representative SEM image shows Au ball bond microcracking along the Au–Al interface after UHAST 2,000 h)

Failure analysis and mechanisms of Au and Cu ball bonds

Unbiased HAST

Typical failure mechanisms of both unbiased HAST (UHAST) of gold (Au) and copper (Cu) ball bonds are IMC microcracking along the Au–Al and Cu–Al interfaces. The stress-induced microcracking occurs in the event of Au and Cu ball bond corrosion in high temperature and moisture environment (130 °C, 85%RH). Insulative corrosion products will cause high resistance or open failure after long durations of UHAST stressing. Figure 3 shows representative Cu ball bond microcracking and opening after 3,000 h in UHAST.

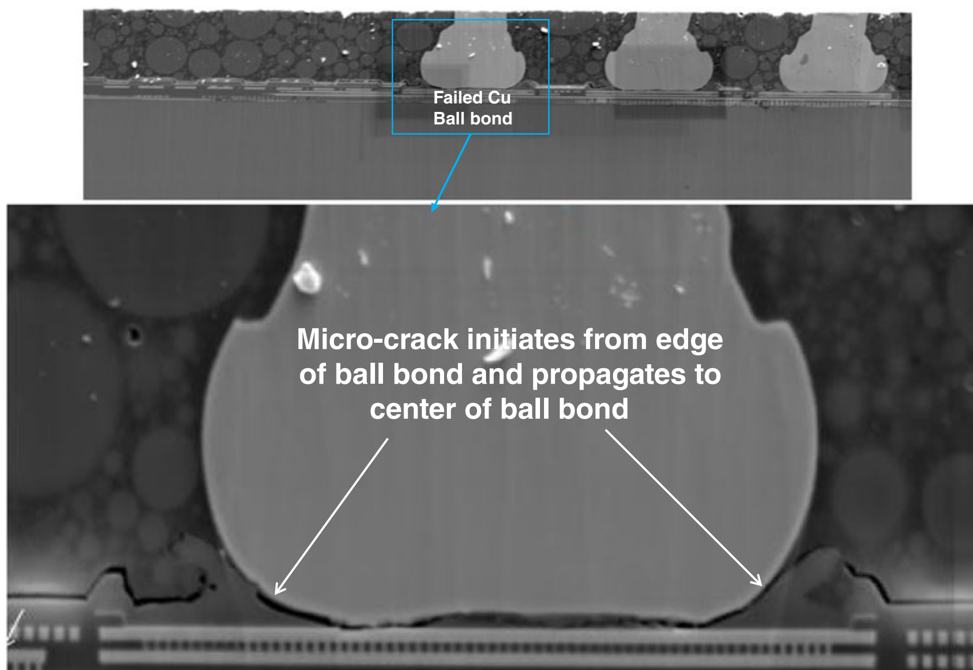

Fig. 6 The representative SEM image shows that Cu ball bond microcracking starts from the edge of the Cu ball bond (larger gapping) toward the center of the ball bond (narrower gapping)

We observed that the crack starts from the edge of Cu ball bonds, and it might propagate toward the center of the ball bond (see Fig. 6).

Figure 4 shows the proposed Cu ball bond corrosion mechanism in the UHAST test. The proposed corrosion mechanism is described in Eqs. 1 to 3 below.

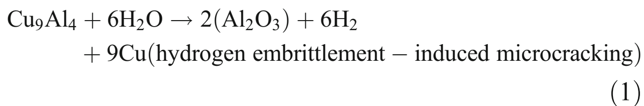

$$Cu_9Al_4 + 6H_2O \rightarrow 2(Al_2O_3) + 6H_2 + 9Cu(\text{hydrogen embrittlement} - \text{induced microcracking}) \quad (1)$$

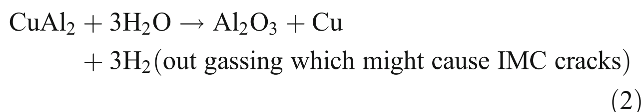

$$CuAl_2 + 3H_2O \rightarrow Al_2O_3 + Cu + 3H_2(\text{out gassing which might cause IMC cracks}) \quad (2)$$

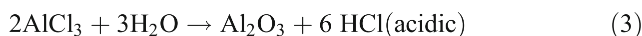

$$2AlCl_3 + 3H_2O \rightarrow Al_2O_3 + 6\ HCl(\text{acidic}) \quad (3)$$

Cu ball bond corrosion is most probably attributed to Cl^- attacking the edge of Cu ball bond region. Hydrolysis of

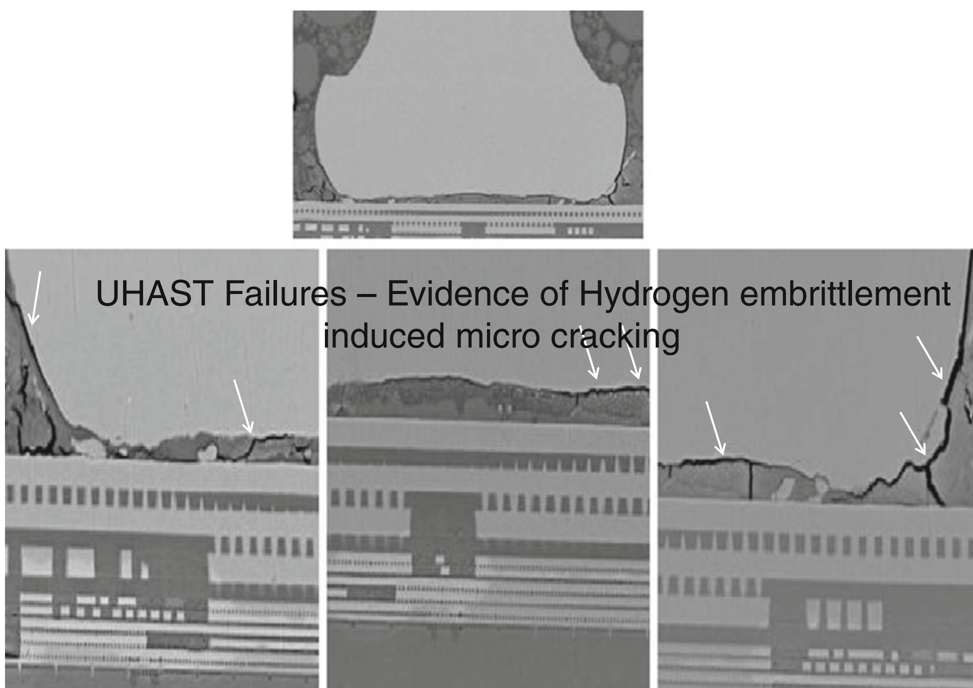

Fig. 7 The SEM image shows that the Cu ball bond opens after the UHAST test. *Arrows* indicate the evidence of possible hydrogen embrittlement-induced microcracking (between Cu to CuAl IMC) which started from the edge of the Cu ball bond

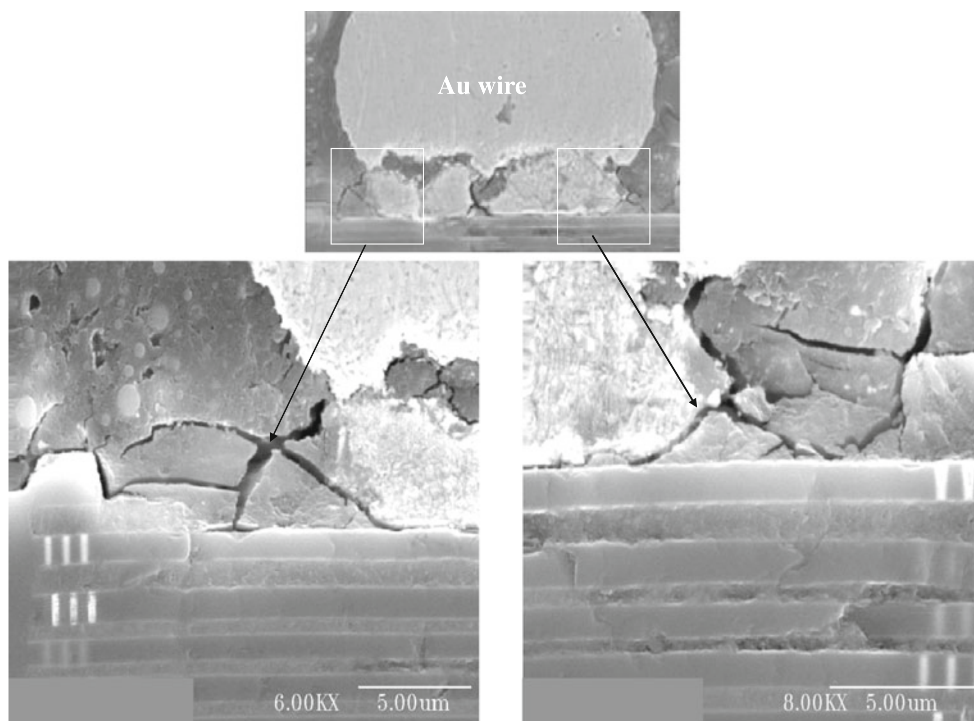

Fig. 8 The SEM image shows that in the microstructural analysis, the Au ball bond opens after the UHAST test. A thicker AuAl IMC is observed compared to CuAl IMC in the Cu ball bond

IMC and $AlCl_3$ (intermediate product) under moisture environment forms aluminum (III) oxide which is a resistive layer, and ionic Cl^- is usually found at the corroded ball bond [1, 10]. Equation 1 indicates the hydrolysis of Cu_9Al_4 into Al_2O_3 and out gassing. Cracking of the Al_2O_3 interface of Cu to the Cu IMC might be due to out gassing of H_2 during hydrolysis (as shown in Eqs. 2 and 3) in between the Cu IMC and Cu ball bonds. Cracking usually starts at the Cu ball bond periphery, and it will propagate toward the center of the Cu ball bond [9, 10, 13]. There is a possibility that under moist conditions, internal oxidation of intermetallic phases can result in oxidation of aluminum, precipitation of the noble metal (Au or Cu), and generation of hydrogen. Possible reactions (not necessary correct) resulting in formation of aluminum oxide that might occur with gold and copper ball bonds are given in Eqs. 4 and 5 [11, 12]. Hydrogen gas evolution due to moisture in contact with intermetallics has been extensively documented and is one of the known causes of embrittlement [12].

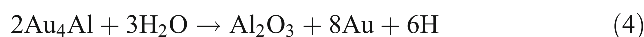

$$2Au_4Al + 3H_2O \rightarrow Al_2O_3 + 8Au + 6H \quad (4)$$

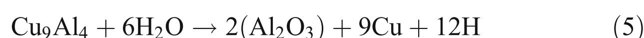

$$Cu_9Al_4 + 6H_2O \rightarrow 2(Al_2O_3) + 9Cu + 12H \quad (5)$$

Au ball bonds also exhibit similar Au oxidation and corrosion during UHAST stress. Figure 5 reveals the

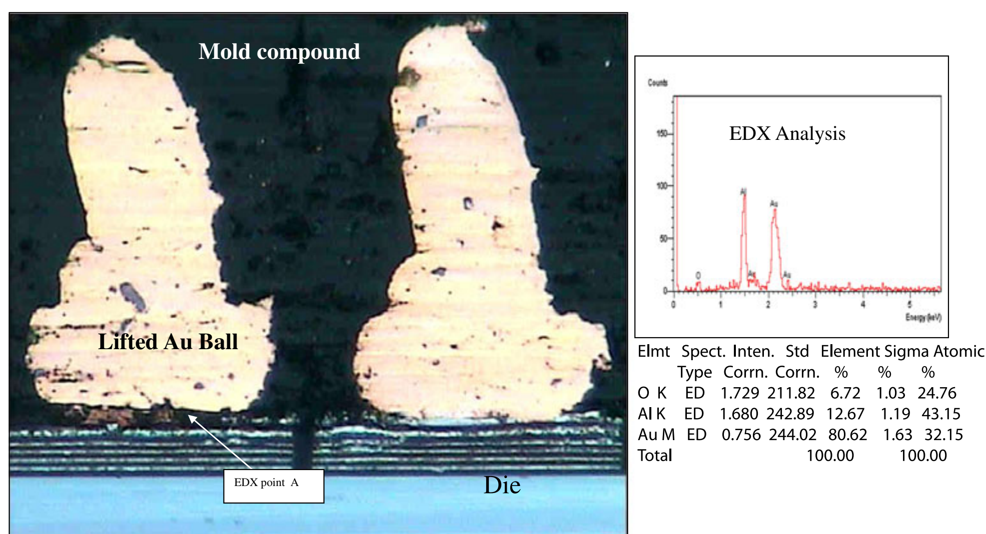

Elmt	Spect. Type	Inten. Corrn.	Std Corrn.	Element %	Sigma %	Atomic %
O K	ED	1.729	211.82	6.72	1.03	24.76
Al K	ED	1.680	242.89	12.67	1.19	43.15
Au M	ED	0.756	244.02	80.62	1.63	32.15
Total				100.00		100.00

Fig. 9 The optical image shows that the lifted Au ball bond opens after the UHAST test. The EDX analysis on the failed Au ball bond indicates the presence of O, Al, and Au elements. The presence of O element proves oxidation of AuAl IMC under moist UHAST environment

Elmt	Spect. Type	Inten. Corrn.	Std Corrn.	Element %
O K	ED	0.838	0.52	6.85
Al K	ED	0.351	0.83	5.56
Si K	ED	0.428	0.91	1.68
Cl K	ED	0.605	0.94	0.24
Cu K	ED	0.970	1.00	79.41
Ta M	ED	0.367	0.77	6.27
Total				100.00

* = <2 Sigma

Fig. 10 Microstructural analysis of the Cu ball bond, which opens after the UHAST test. The EDX analysis on the failed Cu ball bond indicates the presence of O, Cu, Si, Ta, and Cl elements. The presence of O and Cl elements proves internal oxidation of Cu–Al IMC under moist UHAST environment and corrosion by Cl^- ion

representative SEM image of Au ball bonds and microcracking after UHAST 2,000 h. Au is well known for its corrosion resistance compared to Cu ball bonds and is being deployed in microelectronic packaging for more than 25 years.

Microstructural analysis of failed ball bonds

The Au and Cu ball sample which failed to open after UHAST test has been subjected to detailed microstructural analysis such as cross-section and EDX analyses. Figure 6 reveals that the microcrack starts from the edge of the Cu ball bond (with larger gapping of microcrack) and propagates toward the center of the Cu ball bond.

Table 5 EDX analysis of failed Cu and Au ball bonds after the UHAST test

Location	Element (atomic %)						
	Au	Cu	O	Al	Si	Ta	Cl
Au ball	32.15	–	24.76	43.15	–	–	–
Cu ball	–	79.41	6.85	5.56	1.68	6.27	0.24

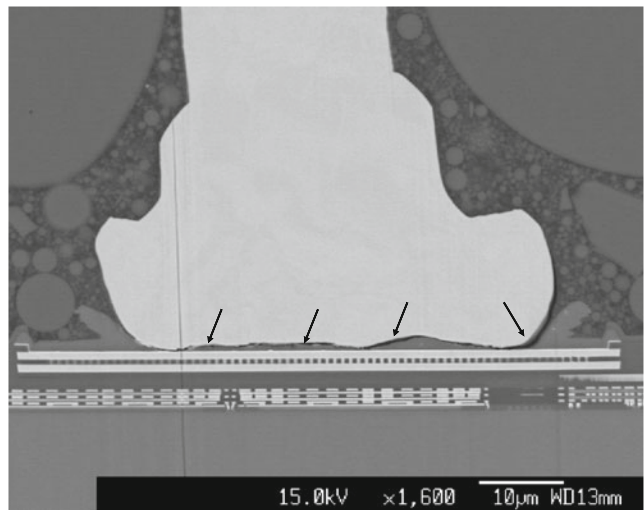

Fig. 11 Representative SEM image of Cu ball bond CuAl interfacial microcracking after TC 9,500 cycles

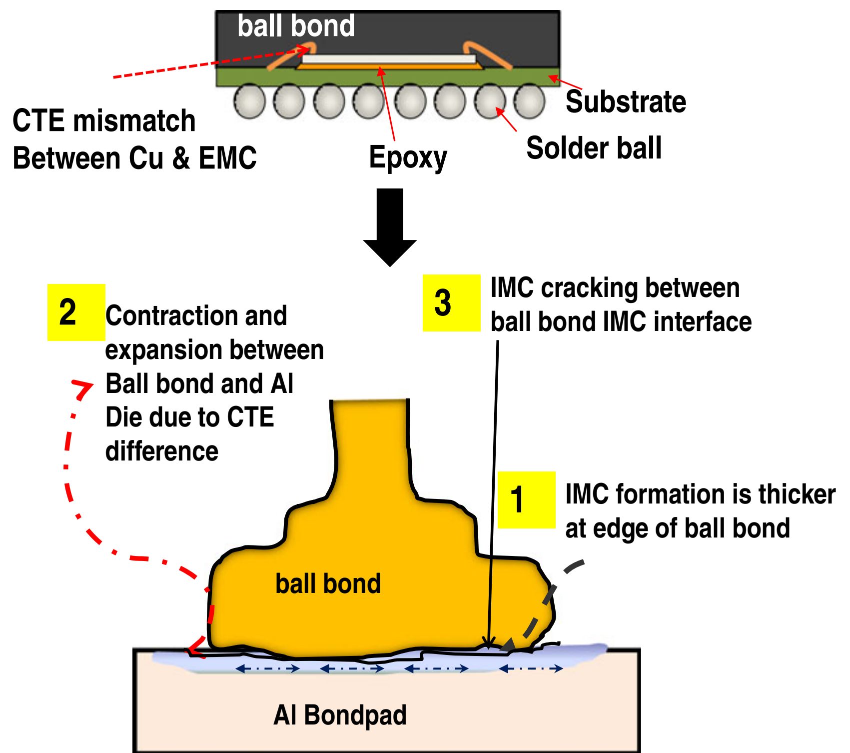

Fig. 12 Proposed TC failure mechanism of Cu ball bond

We have proposed the possible failure mechanism of Cu ball bond under moist UHAST conditions in which the hydrogen out gassing might possibly induce microcracking (hydrogen embrittlement-induced microcracking). Figure 7 shows the microstructure of failed Cu ball bonds with fine microcracking beneath Cu ball bonds.

Au ball bonds undergoing extended hours of UHAST test might fail owing to internal Au IMC oxidation, and microcracking will occur. Figure 8 indicates that the representative Au ball bond which is observed with thicker AuAl IMC failed UHAST and microcrack occurs beneath the Au ball bond.

EDX analysis has been performed on failed Au ball bonds (in Fig. 9) and Cu ball bonds (in Fig. 10), respectively. A large amount of O peak is found for the failed Au ball bond, which is proven with the proposed failure mechanism of Au ball bond whereby a possible internal AuAl IMC oxidation occurred under the UHAST test and led to open failure.

Figure 10 shows the FIB cross-section and EDX analyses of the failed Cu ball bond. The EDX analysis on the microcrack at the edge of the Cu ball bond indicates the presence of O and Cl peaks. This proves that the hydrolysis of CuAl IMC under UHAST moist conditions and Cl peak originates from $AlCl_3$. The trace Cl^- is usually found in epoxy mold compound. Table 5 tabulates the summary of the EDX analysis of Au and Cu ball bonds.

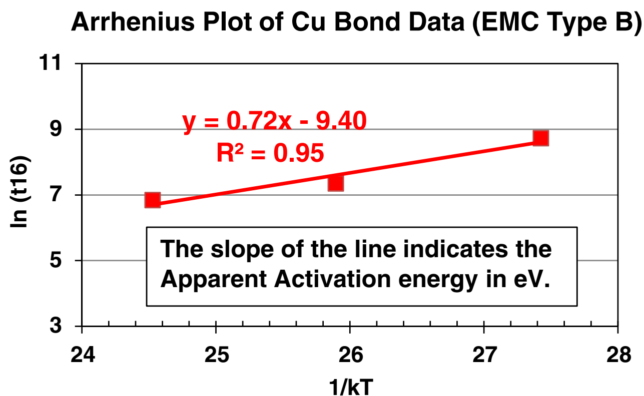

Fig. 13 Arrhenius plot of the Cu ball bonds in FBGA 64 package with EMC type B

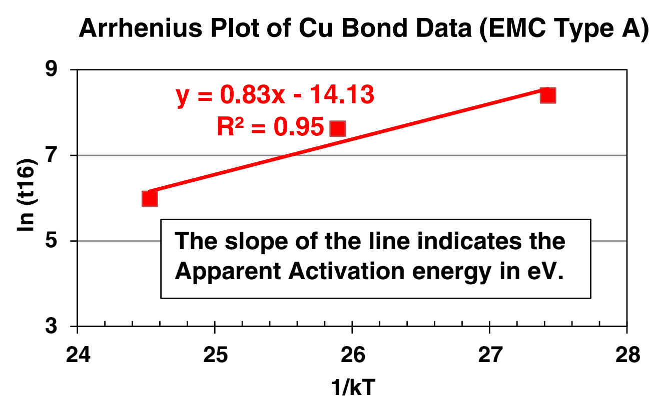

Fig. 14 Arrhenius plot of the Cu ball bonds in FBGA 64 package with EMC type A

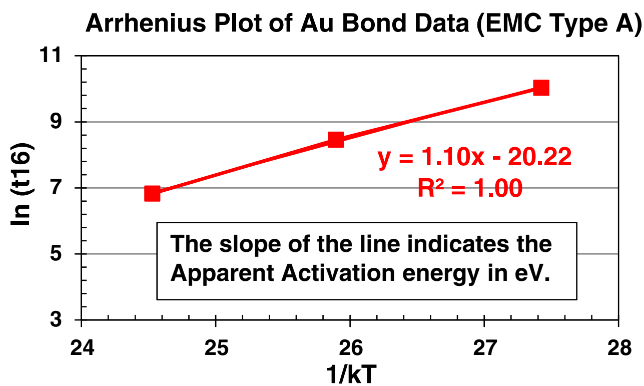

Fig. 15 Arrhenius plot of Au ball bonds in FBGA 64 package with EMC type A

Temperature cycling

Temperature cycling is conducted on the four legs of Au and Cu ball bonds assembled with different EMCs to examine their thermomechanical reliability performance. The mismatch in CTE between the Cu (17 ppm/°C) and Au ball bonds (14 ppm/°C) to the silicon die (3.0 ppm/°C) induced different thermal expansions and contraction rates in the temperature cycling test. The CTE mismatch between the Au and Cu ball bonds with Al bondpad of silicon die will impose different thermal expansion rates during hot cycles (150 °C) and contraction rates during cold cycles (-40 °C). IMC formation started at the edge of the ball bond (due to the ball bond pressing force by capillary), and microcracking will be induced after long cycles of thermal cycling effects. The microcracking occurs in between ball bond IMCs (as shown in Fig. 11).

Figure 12 illustrates the typical package failures induced by TC stress due to CTE mismatch in Au and Cu ball bonds onto Al bondpad metallization.

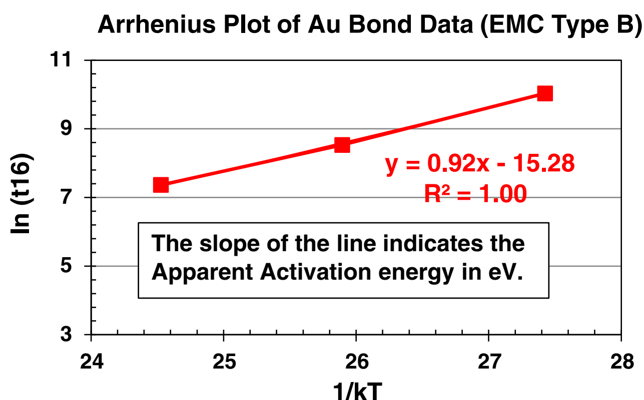

Fig. 16 Arrhenius plot of Au ball bonds in FBGA 64 package with EMC type B

High-temperature storage life

The required activation energies (E_{aa}) of interdiffusion of Cu and Au atoms in Al were modeled by using Arrhenius model after the HTSL test. The fundamental basis of thermal activation is based on the probability of ascending a potential energy barrier due to Maxwell–Boltzmann energy distribution. This physical explanation was actually anticipated by Arrhenius work on chemical reaction rates, in which one would simply substitute the Rydberg gas constant for the Boltzmann constant and use different units. Thermally activated processes are modeled by Arrhenius equation, and it is given in Eqs. 6 and 7.

$$\mathrm{Rate} = \mathrm{R_o} \times \exp(-\mathrm{E_{aa}}/\mathrm{kT}) \tag{6}$$

$$\mathrm{Or\ Rate} = \mathrm{R_o} \times \exp(-\mathrm{E_{aa}}/\mathrm{RT}) \tag{7}$$

where R_o is the rate constant characteristics of infinite temperature, E_{aa} refers to apparent activation energy in electronvolts per atom for physics units or kilocalories per mole for chemical units, k is the Boltzmann constant (8.62×10^{-5} eV/kelvin), R is the Rydberg gas constant (23,063 cal/mol kelvin), and T is the temperature in kelvin.

Using Eq. 7, the acceleration factor AF for T_1 versus T_2 is as follows (in Eq. 8):

$$\mathrm{AF} = \exp[(\mathrm{E_{aa}}/\mathrm{kT})(1/\mathrm{T_1} - 1/\mathrm{T_2})] \tag{8}$$

It is noted that the acceleration factor is sensitive to the value of the apparent activation energy E_{aa} and the temperature difference. The apparent activation energy E_{aa}, which is temperature dependent, can be determined by plotting graph ln (lifetime of ball bonds) versus $1/kT$ as in Eq. 9. Graph *ln T* (lifetime) versus ($1/T$) can be plotted by using Eq. 10.

$$T = R_o \exp(-E_{aa}/kT) \tag{9}$$

$$\ln\ T = -(E_{aa}/R)(1/kT) + \ln\ R_o \tag{10}$$

where self-diffusion coefficient Ro is a constant, E_{aa} is the activation energy in electronvolts for the diffusion process, R is molar gas constant in joules per mole kelvin, and T is the lifetime of ball bonds. The apparent activation energy E_{aa} can be calculated from the gradient of the plot ln T versus $1/kT$. HTSLs of Au and Cu ball bonds for EMCs A and B were conducted to understand and estimate its apparent activation energy (E_{aa}) after long duration of high-temperature bake. Previous studies show that the E_{aa} values of the Au ball bond range from 1.00 to 1.50 eV [15, 25], while the Cu ball bond is about 0.70 eV [14]. In our study, the E_{aa} values obtained are 0.72 eV (in Fig. 13) and 0.83 eV (in Fig. 14) for Cu wire assembled with EMC B and EMC

Table 6 Summary of E_{aa} and HTSL failure mechanisms from previous studies

Ball bond type	HTSL aging test conditions (°C)	E_{aa} (eV)	Failure mechanism	Reference
Cu	150, 175, 200	0.70	CuAl microcrack	[14]
Cu	N/A	0.75	CuAl microcrack	[25]
Cu	150, 175, 200	0.72~0.83	CuAl microcrack	This work
Au	150, 175, 200	1.00~1.50	Kirkendall void	[15]
Au	N/A	1.00~1.26	Kirkendall void	[25]
Au	150, 175, 200	0.92~1.10	Kirkendall void	This work

A, respectively. A lower E_{aa} is found on the Cu ball bonds compared to the Au ball bonds in the HTSL tests.

The Au wire exhibits higher E_{aa} values in the HTSL tests, with 1.10 eV for EMC A (in Fig. 15) and 0.92 eV for EMC B (in Fig. 16), respectively. The typical failure mechanism of AuAl IMC in the HTSL test is attributed to Kirkendall voiding-induced opens [4, 5, 25]. Cu ball bonds are known with slower CuAl IMC growth rate compared to AuAl IMC, and the failure mechanism in HTSL is slightly different from Au ball bonds in HTSL.

Table 6 tabulates the summary of E_{aa} obtained by previous researchers on Au and Cu ball bonds in HTSL test. The typical failure mechanism of Cu ball bond is CuAl IMC microcracking after long durations of high-temperature bake. Au ball bonds (with faster Au atomic diffusion rate into Al metallization) exhibit Kirkendall microvoiding in AuAl to Al bondpad interface and induce opens. Our study shows the similar observation and findings.

Ball bond lifetime analysis by using E_{aa} (apparent activation energy)

Table 7 shows the lifetime estimate of Cu wire bonding in FBGA package, derived from our experimental data herein, for a number of different market segments and usage models. The computations are based on a 0.1 % failure rate at 175 °C, which are approximately 408 h (for Cu ball bond with EMC A) and 302 h (for Cu ball bond with EMC B) from the data collected and shown in lognormal plot. The operating conditions as well as typical life in the computations in Table 7 were taken from JESD94 [25]. The operating temperatures were obtained from the maximum ambient temperature conditions shown in JESD94. Storage conditions were chosen to be 30 °C uniformly across all applications. The data indicate that for all applications listed, there is more than sufficient reliability margin to meet all listed reliability requirements. Similarly, Au ball bond lifetime can be calculated based on the E_{aa} values obtained. We have calculated the lifetime of Au ball bonds (Au ball bond with EMC A and EMC B, respectively), and the data meet typical lifetime (years) as required in JESD94 standard [25].

Effects of molding compound on extended reliability

The EMCs used in this evaluation are from suppliers A and B. The important material characteristics of the mold compound datasheets are given in Table 4. The only difference between the mold compounds is that they are from different mold compound manufacturers. EMC A exhibits higher hours to failures in UHAST extended reliability for EMC A (Fig. 1) but lower cycles to failures in TC extended reliability tests (Fig. 2) compared to EMC B. In HTSL tests, EMC B shows no significant difference in the apparent activation energy (E_{aa}) value in Cu ball bonds while a much lower E_{aa} value in Au ball bonds (Fig. 13). This proves that the different types of epoxy mold compounds have a significant influence in the HTSL test of Au wire bonding. Au ball bonds are well known for its higher IMC growth rate and increased susceptibility to

Table 7 Lifetime estimations for various market segments (Cu wire bond FBGA package)

Market segment	Typical lifetime (years)	Operating condition		Storage conditions		# of lives (years) Cu EMC A	# of lives (years) Cu EMC B
		Time (h)	Temp. (°C)	Time (h)	Temp. (°C)		
Consumer desktop	5	13,000	30	30,800	30	264.61	51.82
High-end server	11	94,000	30	2,360	30	120.28	23.55
Avionics electronics	23	150,000	50	51,480	30	10.37	2.58
Telecom handheld	5	43,800	40	0	30	96.17	21.47
Telecom controlled	15	131,000	70	400	30	2.20	0.69
Automotive underdash	15	8,200	45	123,200	30	72.55	14.80
Automotive underhood	15	8,200	125	123,200	30	0.73	0.38

Kirkendall microvoiding after the HTSL test compared to slower CuAl IMC growth rate. Hence, we observed no significant E_{aa} values obtained in Cu ball bonds for EMC A and EMC B (Figs. 14 and 13). Both EMCs show promising extended reliability results which far exceed the typical 96 h of UHAST and 1,000 cycles of TC according to JEDEC standards. Hence, both EMC A and B are used in our flash memory BGA laminate.

Effects of wire types on extended reliability

Many previous studies reported Au wire bonding with higher reliability margins compared to Cu wire bonding. However, there are very few published data on extended reliability of Au and Cu ball bonds. In our study, Au ball bonds show higher UHAST reliability compared to Cu ball bond in FBGA package. This is notable as Au is much more stable and has higher corrosive resistance compared to Cu. Cu is easily oxidized and corroded under moist environments, especially in the UHAST or biased HAST tests. Our extended reliability study (Fig. 1) shows similar findings with Au wires in EMC A. Another factor affecting the first ball bond strength is Au wire bond shear or wire pull strength shows less variation compared to Cu ball bonds. This as-bonded stage strength value would influence the reliability of ball bonds in semiconductor packaging.

However, Cu ball bonds exhibit higher cycle to failure in TC test compared to Au ball bonds (Fig. 2) regardless of EMC types. The CTEs of Cu and Au are pretty similar in this case. This is an interesting finding since the reliability performance of TC stress is pretty much material CTE dependent with regard to Al bondpad. The mismatch in CTE between the Cu (17 ppm/°C) and Au ball bonds (14 ppm/°C) to the silicon die (3.0 ppm/°C) induced different thermal expansions and contraction rates in the temperature cycling test. The CTE mismatch between the Au and Cu ball bonds with Al bondpad of silicon die will impose different thermal expansion rates during hot cycles (150 °C) and contraction rates during cold cycles (-40 °C).

Future works and recommendation

Cu wire will be continuously developed to replace Au wire in higher pin counts of semiconductor packages, but transition is predicted to be less on power-device-based packages. Future engineering work should be focused on knowledge-based reliability testing and prediction to understand the initial failure point in semiconductor device packaging. Extended reliability concept would be used in this type of reliability studies. Further characterization should be carried out for Pd–Ag–Au or bare Ag wire bonding in nanoscale device packaging, especially for 45, 28, 22, or subnanoscale 10 nm below technology nodes.

Conclusions

In this research, we analyzed the effects of wire alloy on extended reliability of UHAST, TC, and HTSL stresses. Au ball bonds show a significant higher UHAST reliability compared to Cu ball bond in FBGA package with EMC A. This is notable as Au is much more stable and has higher corrosive resistance compared to Cu. Contrary results occur in TC, where Cu ball bond is more superior compared to Au ball bond. EMC B exhibits higher TC reliability margins compared to EMC A assembled with Au or Cu wires. However, both EMCs are far exceeding the minimum required 96 h of UHAST and 1,000 cycles of TC according to JEDEC standards. The E_{aa} values obtained for Au ball bonds range from 0.92 to 1.10 eV and 0.72 to 0.83 eV for Cu ball bonds. These values are close to previous HTSL studies conducted on Au and Cu ball bonds. Au wire bonding will still remain as a mainstay in microelectronic packaging, especially for more complicated semiconductor packages (with higher pin counts), while Cu wire bonding will equally gain some market shares in low-pin-count and power device packaging. Ag wire bonding would probably become an emerging technology as an option in microelectronic packaging. However, more engineering works should be carried out to understand the extended reliability performance as well as assembly yield monitoring before deployment for high-volume manufacturing. Future engineering work should be focused on knowledge-based reliability testing and prediction to understand the initial failure point in semiconductor device packaging. Extended reliability concept would be used in this type of reliability studies.

Acknowledgments The authors would like to take this opportunity to thank Spansion management (Gene Daszko, Tony Reyes, and Chong HL) for their management support for the paper publication.

Open Access This article is distributed under the terms of the Creative Commons Attribution License which permits any use, distribution, and reproduction in any medium, provided the original author(s) and the source are credited.

References

1. Ellis TW, Bond W (2004) The future of gold in electronics introduction. Gold Bulletin 37:66–71
2. Appelt BK, Tseng A, Chen C-H, Lai Y-S (2011) Fine pitch copper wire bonding in high volume production. Microelectronics Reliability 51:13–20. doi:10.1016/j.microrel.2010.06.006
3. Breach CD (2010) What is the future of bonding wire? Will copper entirely replace gold? Gold Bulletin 43:150–168
4. Breach CD (2009) Intermetallic growth in gold ball bonds aged at 175c: Comparison between two 4 N wires of different chemistry. Gold Bulletin 42:92–105
5. Muller T, Schraplerl L, Altmann F et al (2006) Influence of intermetallic phases on reliability in thermosonic Au–Al wire

bonding. IEEE Electronics System Integration Technology Conference, Dresden, pp 1266–1273
6. Xu H, Liu C, Silberschmidt VV et al (2011) Intermetallics intermetallic phase transformations in AuAl wire bonds. Intermetallics 19:1808–1816. doi:10.1016/j.intermet.2011.07.003
7. Zulkifli MN, Abdullah S, Othman NK, Jalar A (2012) Some thoughts on bondability and strength of gold wire bonding. Gold Bulletin 45:115–125. doi:10.1007/s13404-012-0060-y
8. Gan CL, Toong TT, Lim CP, Ng CY (2010) Environmental friendly package development by using copper wire bonding, In Proceedings of 34th IEEE CPMT IEMT. Malacca 2010:1–5
9. Gan CL, Ng EK, Chan BL et al (2012) Technical barriers and development of Cu wirebonding in nanoelectronics device packaging. Journal of Nanomaterials 2012(173025):1–7. doi:10.1155/2012/173025
10. Gan CL, Ng EK, Chan BL, Hashim U (2012) Reliability challenges of Cu wire deployment in flash memory packaging. IEEE Proceedings of International Microsystems, Packaging, Assembly and Circuit Technology Conference, Taipei, pp 498–501
11. Breach CD, Shen NH, Lee TK, Holliday R (2011) Failure of gold and copper ball bonds due to intermetallic oxidation and corrosion. 18th IEEE International Symposium on the Physical and Failure Analysis of Integrated Circuits (IPFA) 1–6
12. Breach CD, Lee TK (2011) Conjecture on the chemical stability and corrosion resistance of Cu–Al and Au–Al intermetallics in ball bonds. IEEE International Conference on Electronics Packaging Technology and High Density Packaging. 275–283
13. Gan CL, Ng EK, Chan BL, Kwuanjai T, Jakarin S, Hashim U (2012) Wearout reliability study of Cu and Au wires used in flash memory fine line BGA package. IEEE Proceedings of International Microsystems, Packaging, Assembly and Circuit Technology Conference, Taipei, pp 494–497
14. Classe F, Gaddamraja S (2011) Long term isothermal reliability of copper wire bonded to thin 6.5 μm aluminum. IEEE International Reliability Physics Symposium 685–689.
15. Blish RC, Li S, Kinoshita H et al (2007) Gold–aluminum intermetallic formation kinetics. IEEE Transactions on Device and Materials Reliability 7:51–63
16. Gan CL, Ng EK, Chan BL, Classe FC, Kwuanjai T, Hashim U (2013) Wearout reliability and intermetallic compound diffusion kinetics of Au and PdCu wires used in nanoscale device packaging. Journal of Nanomaterials 2013(486373):1–9
17. Cho J, Yoo K, Hong S, et al. (2010) Pd effects on the reliability in the low cost Ag bonding wire. IEEE International Electronic Components and Technology Conference 1541–1546
18. Kai LJ, Hung LY, Wu LW, et al. (2012) Silver Alloy Wire Bonding. pp 1163–1168
19. Pagba A, Reynoso D, Thomas S, Toc HJ (2010) Cu wire and beyond—Ag wire an alternative to Cu? 2010 12th Electronics Packaging Technology Conference 591–596.
20. Tsai HH, Lee JD, Tsai CH, Wang HC, Chang CC, Chuang TH (2012) An innovative annealing twinned Au–Ag–Pd bonding wire for IC and LED packaging, IEEE International Microsystems Packaging Technology Conference 505–508
21. Long Z, Han L, Wu Y, Zhong J (2008) Study of temperature parameter in Au–Ag wire bonding. IEEE Transactions on Electronics Packaging Manufacturing 31:221–226
22. Chuang TH, Chang CC, Chuang CH, Lee JD, Tsai HH (2012) Formation and growth of intermetallics in an. IEEE Transactions on Components, Packaging and Manufacturing Technology 1–7
23. Chuang TH, Wang HC, Tsai CH et al (2012) Thermal stability of grain structure and material properties in an annealing-twinned Ag–8Au–3Pd alloy wire. Scripta Materialia 67:605–608. doi:10.1016/j.scriptamat.2012.06.022
24. JEDEC JEP 122 (2010) Failure mechanisms and models for semiconductor devices
25. JEDEC JESD94 (2008) Application specific qualification using knowledge based test methodology